IB05

19th International Symposium of Ballistics, 7–11 May 2001, Interlaken, Switzerland

DEVELOPMENT AND VALIDATION OF A COMPREHENSIVE MODEL OF THE PLASMA JET GENERATED BY AN ELECTROTHERMAL-CHEMICAL IGNITER

M.J. Nusca, M.J. McQuaid and W.R. Anderson

Weapons and Materials Research Dir., Army Research Laboratory, APG, MD, USA

The US Army Research Laboratory is investigating the Electrothermal-Chemical (ETC) gun concept and has undertaken a comprehensive study of the interaction of the plasma efflux from an ETC igniter with solid propellant grains. The goal of this work is to elucidate the physical, mechanical, and chemical mechanisms that underlie the favorable ballistic effects observed in ETC guns. This paper describes the first phase of the modeling effort in support of the project. A time-accurate computational fluid dynamics code is used that includes high-temperature thermodynamics, variable specific heats and transport properties, and finite-rate chemical kinetics. Validation of this code utilizes experiments with an ETC igniter fired into open-air, generating an unsteady flow that impinges on an instrumented plate. Computer simulations reveal gas dynamic and chemical details of the plasma jet as it mixes with air and interacts with the plate, representing a unique model of the ETC plasma.

INTRODUCTION

Future military engagements will require weapons systems exhibiting improved range and accuracy. One of the technologies under investigation to achieve these goals is the Electrothermal-Chemical (ETC) propulsion concept. In the ETC gun, energy, which is stored either in batteries or a rotating device, is converted on demand into an electrically generated plasma (resulting from the ablation of polyethylene material in a capillary) that is injected into the chamber in a howitzer or gun. This plasma energy is used to ignite the chemical propulsion charge (i.e., solid propellant) as well as to enhance gun performance by taking advantage of a number of unique plasma characteristics. For example, a low density plasma jet can efficiently ignite charges of high loading density, can control propellant mass generation rates [1], can reduce propellant charge temperature sensitivity, i.e., the variation of gun performance with changing ambient temperature [2,3] and can shorten ignition delay, i.e., the time interval between firing of the igniter and ignition of the propellant [4]. Since a plasma has a much lower density than the gases generated by a chemical igniter it has been suggested that energy transport by convection may be as important as radiation transport in plasma-propellant interactions [5,6]. In addition, the

plasma is at a temperature that is considerably higher than conventional chemical igniters thus, radiation effects are nearly 100 times greater than that of chemical igniters (i.e., a T^4 effect).

All of these effects can lead to significant changes in ballistic behavior and useful improvements in gun performance. The goal of research in this area is to elucidate the relevant physical, mechanical, and chemical mechanisms that underlie the observed ballistic effects. The first phase of the modeling effort involves a time-accurate computational fluid dynamics (CFD) code which has been written to include high-temperature thermodynamics, variable specific heats and transport properties (viscosity and thermal conductivity), and finite-rate (nonequilibrium) chemical kinetics (the mechanism is described in Ref. 7). A separate capillary model [8] supplies boundary conditions for the CFD code in terms of the physical and chemical properties of the plasma capillary efflux. Validation of the capillary model and the CFD code, including coupled chemistry, is conducted by simulating a series of experiments [9] wherein a plasma jet is generated from a plasma cartridge; pressures in the resulting unsteady flow field are measured using probes mounted on a plate held normal to the efflux.

EXPERIMENTAL EFFORT

Litzinger et al. [9] at Penn State University (PSU) have designed and operated the open-air experiment shown schematically in Figure 1. The polyethylene capillary is typically 26 mm in length and 3 mm in diameter (d). An extension tube 26 mm in length is placed at the capillary exit, which guides the plasma efflux into the open-air. The capillary and the extension tube are mounted within a solid housing (not shown in Figure 1). An instrumented plate is placed at some distance (L) from the plasma device, typically 19 mm. Pressure probes are mounted on the plate with a spacing of 9.53 mm (3/8 inches).

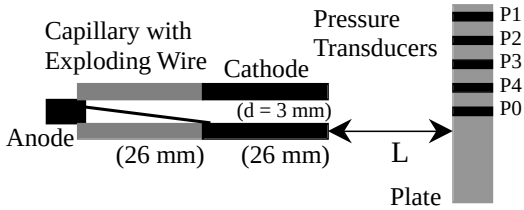

Figure 1. Schematic of the Penn State University (PSU) experimental setup.

MULTI-SPECIES REACTING FLOW CFD CODE

The high-temperature, non-ideal, chemically reacting gas flow field within the capillary efflux jet is numerically simulated using CFD. The NSRG2 code, written by the first author [10], solves the 2D/axisymmetric, unsteady, real-gas Navier-Stokes equations including submodels that represent finite-rate (nonequilibrium) chemical reactions, multi-

species diffusion, as well as variable specific heats, viscosity and thermal conductivity. The Navier-Stokes equations for 2D/axisymmetric (x,y coordinates) reacting (N species) and unsteady (time, t) flow are written in nondimensional array form.

$$\frac{\partial U}{\partial t}+\frac{\partial F}{\partial x}+\frac{\partial G}{\partial y}+H=0 \tag{1}$$

The dependent variables are density (r), velocity (V and components u,v), energy (e), and species mass fraction (c_i); note that α is the flag for two-dimensional, 0, and axisymmetric, 1, flows.

$$U=\left\{\rho\ y^{\alpha},\rho\ u\ y^{\alpha},\rho\ v\ y^{\alpha},\rho\ e\ y^{\alpha},\rho\ c_1\ y^{\alpha},\ldots\ldots\ldots,\rho\ c_N y^{\alpha}\right\}$$

The F and G arrays contain flux terms (convective and diffusive), heat transfer terms and stress terms (normal and shear) [10,11]. The H array contains source terms such as normal stresses (σ+) and the chemical production terms (w_i) for each specie.

$$H=\left\{0,0,\alpha\sigma_{+},0,-\dot{w}_1,\ldots\ldots\ldots,-\dot{w}_N\right\}$$

The chemical production terms are computed using a chemical kinetics mechanism developed specifically for plasma/air chemistry [7]. The mechanism consists of 57 reactions and 39 species: electrons, C, C^+, C^{++}, C^-, CH, CH^+, CN, CN^+, CO, CO^+, C_2, C_2^+, H, H^+, H^-, H_2, H_2^+, N, N^+, NH, NH^+, NO, NO^+, N_2, N_2^+, O, O^+, OH, OH^+, O_2, O_2^+, H_2O, HO_2, H_2O_2, HNO_2, NO_2, CO_2 and O_3. An important simplifying assumption was made in constructing this mechanism, namely only mixtures which had a concentration of O_2 much greater than that of the plasma constituents were considered. As a result the mixtures were assumed to be fuel lean in the combustion sense, the C and H containing species mentioned above being fuels.

Since no provisions have been made in the conservation equations (Eq. 1) for flows with electric currents, the flowfield was rendered electrically neutral by setting the diffusion velocity of the electrons equal to the average diffusion velocity of the ions; the diffusion coefficient for the electrons is then computed from that of the ions. We realize that the plasma gas does not necessarily behave as a perfect fluid. Indeed the ionized gas is usually characterized as rarefied and one in which Coulomb interactions between charged particles create significant departures from the perfect gas behavior. However, for “weakly” imperfect gases one can prescribe terms that account for Coulomb interactions as corrections to the classic pressure-density-temperature relations. Such corrections are described in Reference 8. Alternately, it has been shown [12] that the property determinations obtained from the NASA-Lewis database [13] without modification, such as the enthalpy and specific heats, are reasonably accurate and that the correction terms need not be employed.

The Navier-Stokes equations (Eq. 1) are written in integral form and then re-expressed in a semi-discrete fashion using a finite-volume discretization technique. The numerical computations proceed by solving the semi-discrete equation on each computational cell using central and upwind numerical differences along with flux-limiting. Once properly discretized, the resulting set of algebraic equations are solved in a coupled manner

in time using an explicit time-accurate method. The numerical time step is computed using the CFL condition. A separate chemical time step is computed as well. The final time step is based on the smallest of these. For a more complete description of the numerical scheme, the reader is referred to papers by Nusca [10,11].

RESULTS AND DISCUSSION

The computational domain chosen to simulate the PSU experiment is shown in Fig. 2a. This domain extends from the capillary/extender-tube on the left to the plate on the right (19 mm) and from the centerline of the capillary (and plate) to a fixed radial distance (40 mm) which is determined by the distance from the plate centerline to the pressure probe designated P1 and includes a small radial distance beyond. This region was discretized using 154 axial grid cells and 295 radial grid cells, distributed with essentially even spacing throughout as shown in Fig. 2a (partial grid shown for clarity). Some degree of radial grid clustering was used up to .015 m in order to more accurately resolve the formation of important gas dynamic phenomena (expansions, shocks and turbulent mixing). The boundary conditions for the region are symmetry on the axis (Y=0), outflow at Y= .04 m, no-slip/no-penetration on the capillary housing surface (X=0, .0015 < Y < .04 m) and on the plate surface, specified inflow at the capillary exit (X=0, 0 < Y < .0015 m). Initially, the entire flow field is filled with air (.8 mole fraction of N_2 and .2 mole fraction of O_2). Fig. 3a shows the current amplitude variation for a typical experiment. Given the amplitude/time and the physical characteristics of the capillary, the capillary model [8] generates the range of density (Fig. 3b, solid line), velocity (Fig. 3b, dashed line), pressure, temperature and species distributions (pressure and temperature variations have peak values of 33 MPa and 30,000 K, respectively). The inflow conditions for the computational domain follow from these values.

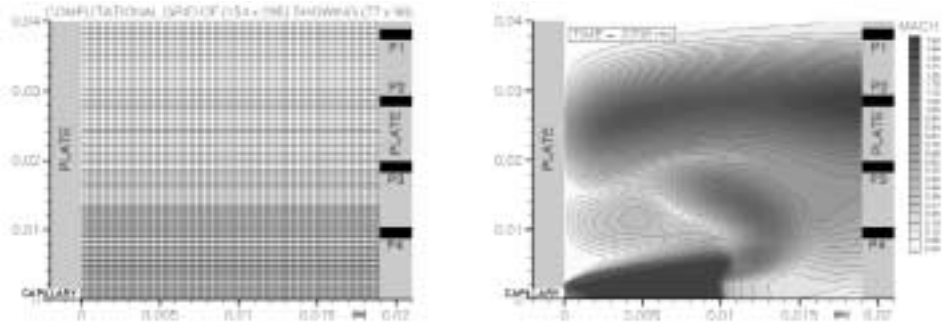

Figure 2. a) Computational grid. b) Computed mach number contours.

The low density and high pressure plasma efflux enters the open-air as a highly underexpanded jet (see gray-scale contours in Fig. 2b with Mach numbers between 0, white, and 1.5+, black). Fig. 4a shows a schematic of the gas dynamic features expected in such a flowfield. The efflux of plasma from the inlet generates a weak precursor shock (A) that extends spherically. Behind this shock is air; the plasma is entirely contained by this

shock and is separated from the air by an irregularly shaped contact surface (B) across which pressure and velocity are preserved but entropy changes discontinuously. Expansion waves, generated at the inlet (C), travel to the precursor shock (A), are reflected as weak compression waves, and coalesce into a strong oblique shock, or barrel shock (D). This barrel shock (D) terminates in an irregular reflection that forms a triple-point (E) joining the barrel shock (D) it's reflection (F), and a normal shock (G) or Mach disk. Whereas the precursor shock (A) is relatively weak, producing a mildly supersonic flow, the barrel shock (D) and Mach disk (G) are strong shocks that enclose a fully supersonic flow.

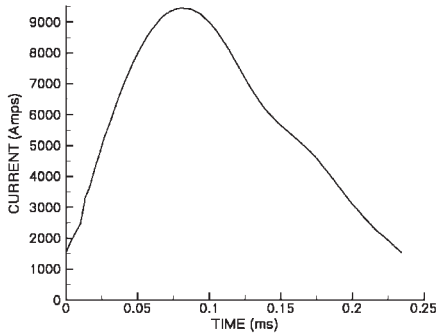

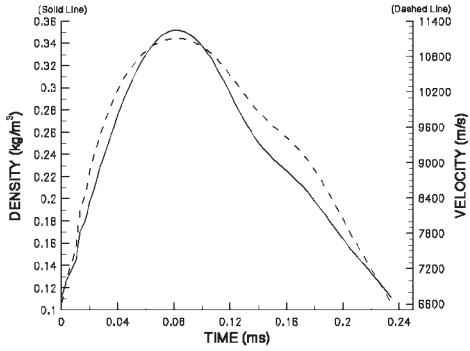

Figure 3. a) Current history. b) Efflux density and velocity histories.

By about 0.07 ms (Fig. 2b) the predominant gas dynamic features in the underexpanded jet have been formed and the precursor shock is traversing the plate vertically. Due to the variable viscosity in the flowfield the precursor shock is more diffuse than the Mack disk or the barrel shock. The precursor shock reaches the plate at about 0.05 ms. Stagnation of supersonic flow on the plate causes a shock reflection that moves back toward the capillary as the precursor shock travels along the plate. This causes the Mack disk to recede, settling at a position 0.01 m from the capillary (Fig. 2b).

Fig. 4b displays the computed and measured pressure peaks (maximums) on the plate and the corresponding time-of-arrival of the precursor shock. The computed results for a 19 mm standoff of the plate (▲ and solid line) compare well with the measured values (▲ and dashed line). In general, the computed shock velocity is too high, perhaps due to the absence of capillary residue (i.e., particles from the vaporization of the polyethylene liner) in the simulation. The translation of these particles would remove energy from the flow and reduce the mean velocity. This would explain the overprediction of peak pressures at the P4 tap location, where most of the particles are usually found to accumulate. Fig. 5 shows the typical comparison for the P4 and the P1 tap locations. Predicted results for the P4 tap location (Fig. 5a) have been shifted in time by 0.022 ms in order to line up the arrival time for the precursor shock.

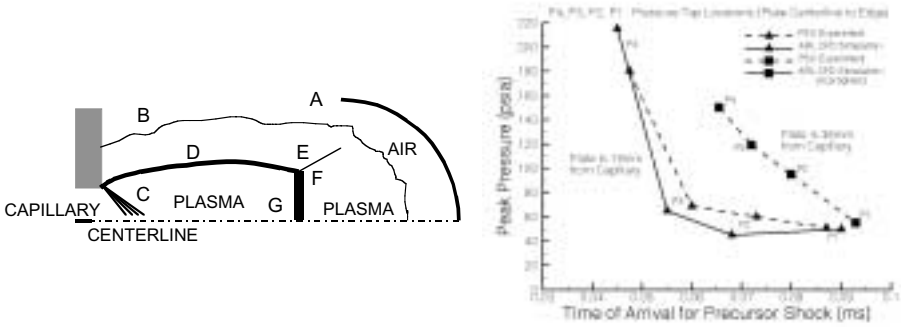

Figure 4. a) Higly unterexpanded jet. b) Peak pressure data/computations.

With this adjustment, the timing of subsequent pressure peaks are well predicted by the code, but the pressure levels are too low. The results for the P1 tap location are also encouraging (no adjustments have been made) since the pressure peaks occur at regular time intervals for both predicted and measured data; however, the predicted pressures are too high. Fig. 6 displays some of the chemical aspects of the flowfield. Fig. 6b shows the time histories of the major species at the plate centerline (i.e., P0 tap location). Comparison of this figure with Fig. 6a (distributions at the capillary exit) indicates that a large proportion of the ion species are actually deposited onto the plate which are expected to ultimately affect the ignition and combustion characteristics of propellant. Of course, these results are dependent on the plasma/air chemical mechanism [7] employed in this study and therefore warrant further study. See Reference 11 for a presentation and discussion of the complete set of computational results.

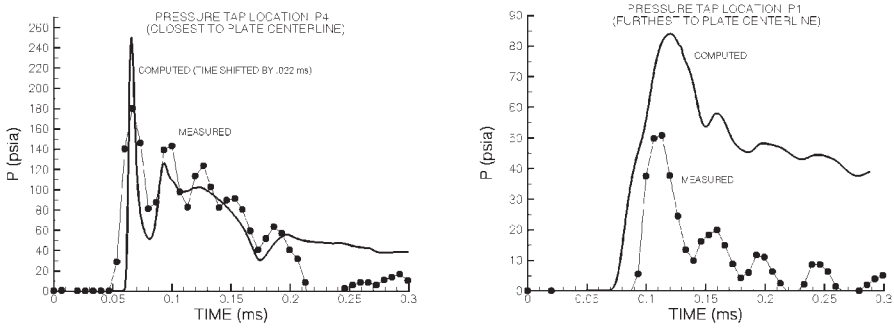

Figure 5. Computed and measured pressure histories at taps P4 (a) and P1 (b).

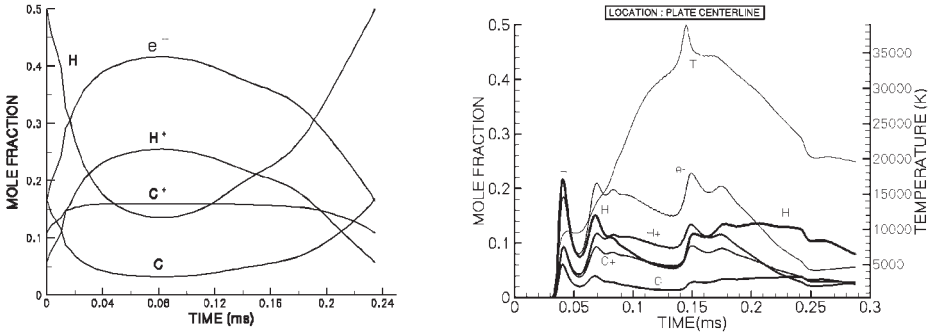

Figure 6. Computed mole fractions; a) capillary exit b) plate centerline.

CONCLUSIONS

A time-accurate CFD code has been applied to the modeling of the high temperature, chemically reactive plasma efflux from an ETC igniter fired into open-air and impinging on an instrumented plate. The major features of this efflux have been resolved by numerical simulation revealing a highly underexpanded jet with a strong precursor shock, a barrel shock that reflects at a triple-point, and a Mach disk. Impact of the jet upon a plate generates a stagnation region, a reflected shock that travels back toward the capillary, and a normal shock that traverses the plate. Evidence of these phenomena is seen in both the experimental data and the prediction. The presence of these shocks has important implications for mechanical damage to solid propellant exposed to the plasma efflux. Chemical conditions at the plate are quite different from those at the ETC igniter. The model indicates that ions are present at the plate and that mixing (and reaction) between the plasma species and the air is present in a narrow region near the efflux jet.

REFERENCES

1. Del Guercio, M., "Propellant Burn Rate Modification by Plasma Injection," *Proceedings of the 34th JANNAF Combustion Meeting*, CPIA Publication 662, Vol. 1, pp. 35–42, October 1997.
2. Perelmutter, L., Sudai, M., Goldenberg, C., Kimhe, D., Zeevi, Z., Arie, S., Melnik, M. and Melnik, D., "Temperature Compensation by Controlled Ignition Power in SPETC Guns," *Proc. of the 16th International Symposium on Ballistics*, pp. 145–152, September 1996.
3. Dyvik, J.A. and Katulka, G., "ETC Temperature Compensation; Experimental Results of 120-mm Test Firings," *Proc. of the 33rd JANNAF Comb. Mtg*, CPIA Pub. 653, Vol. 3, pp. 111–119, Nov.1996.
4. Katulka, G.L., and Dyvik, J., "Experimental Results of Electrical Plasma Ignition in 120-mm Solid Propellant Tank Gun Firings," *Proc 33rd JANNAF Comb. Mtg*, CPIA Pub. 653, Vol. 3, Nov. 1996.
5. Nusca, M.J. and White, K.J., "Plasma Radiative and Convective Interactions with Propellant Beds," *Proceedings of the 34th JANNAF Combustion Mtg*, CPIA Pub. 662, Vol. 1, pp. 21–42, October 1997.
6. White, K.J., Williams, A.W., and Nusca, M.J., "Plasma Output and Propellant Radiation Absorption Characteristics," *Proc. of the 35th JANNAF Comb. Mtg*, CPIA Pub. 680, Vol. 1, pp. 237–246, Dec. 1998.
7. Anderson, W.R., and Schroeder, M.A., "Chemical Mechanism for ETC Plasma Interaction with Air," *Proceedings of the 36th JANNAF Combustion Meeting*, CPIA Pub. 691, Vol.2, October 1999, pp. 43–54.
8. McQuaid, M.J., and Nusca, M.J., "Calculating the Chemical Compositions of Plasmas Generated by an Ablating-Capillary Arc Ignition System," *Proc. of the 36th JANNAF Comb. Mtg*, CPIA Pub. 691, Vol. 2, Oct. 1999, pp. 143–158 (also, ARL-TR-2046, US Army Research Laboratory, APG, MD, 1999).
9. Litzinger, T.A., Li, J-Q, Zhou, H., Kudva, G., and Thynell, S., "Plasma Propellant Interactions: Experiments and Modeling," *Proc. of the 37th JANNAF Combustion Meeting*, CPIA, November 2000.
10. Nusca, M.J., *Numerical Simulation of Electromagnetic Wave Attenuation in Nonequilibrium Chemically Reacting Flows, Computers and Fluids*, Vol. 27, No. 2, 1998, pp.217–238.
11. Nusca, M.J., McQuaid, M.J., and Anderson, W.A., "Development and Validation of a Multi-Species Reacting Flow Model for the Plasma Jet Generated by an ETC Igniter," *Proc. of the 37th JANNAF Comb. Subcom. Mtg., in press, Nov. 2000.*
12. McQuaid, M.J., and Nusca, M.J., "Thermodynamic Property Characterization of Plasmas Generated by an Ablating-Capillary Arc," *Proc. of the 37th JANNAF Combustion Subcommittee Mtg*, Nov. 2000.
13. McBride, B.J., and Gordon, S., *Computer Program for Calculation of Complex Chemical Equilibrium Compositions and Applications, II. Users Manual and Program Description*, NASA RP 1311, June 1996.